PAPER • OPEN ACCESS

Electrochemical contrast switching between black and white appearance of gelatin-covered zinc

To cite this article: Agnieszka Natalia Ksiazkiewicz *et al* 2020 *J. Phys. Mater.* **3** 025009

View the article online for updates and enhancements.

Journal of Physics: Materials

PAPER

Electrochemical contrast switching between black and white appearance of gelatin-covered zinc

Agnieszka Natalia Ksiazkiewicz[1] , Christian Fernández-Solis[1] and Andreas Erbe[1,2,3]

[1] Max-Planck-Institut für Eisenforschung GmbH, Max-Planck-Str. 1, 40237 Düsseldorf, Germany
[2] Department of Materials Science and Engineering, NTNU, Norwegian University of Science and Technology, 7491 Trondheim, Norway
[3] Author to whom any correspondence should be addressed

E-mail: gelatin-zn-electrochem@the-passivists.org

Abstract

Zinc and its alloys are widely used in the surface protection of metallic structural materials. Thus, zinc is an interesting and relevant candidate material for preparing stimuli-responsive surfaces. In this work, the switching of the optical appearance of zinc between black and white by an applied electrode potential is demonstrated. The zinc surface was covered by gelatin films and subjected to cyclic voltammetry (CV) in a chloride-containing electrolyte which induced pitting corrosion on the zinc surface. Between the different parts of the CV cycles, a reversible change in optical appearance was observed. During the oxidative half-cycles, the surfaces appear white, and during the reductive half-cycles, the surfaces appear brown to black, i.e. dark. Surface characterisation by x-ray photoelectron spectroscopy (XPS) and infrared (IR) spectroscopy shows that the gelatin coating is slightly oxidised during intial stages of the process, but remains intact and present at the surface. Raman spectra prove the presence of ZnO at the interface. Surface analysis shows only minor differences in composition between the black and white surfaces. Based on the available characterisation data, the white appearance associated with anodic currents is attributed to the formation of a non-passivating ZnO. The black appearance associated with cathodic currents is attributed to reduction of surface-confined zinc species, including ZnO and Zn^{2+}. The role of the gelatin is presumably to prevent diffusion of the dissolution products into solution by complex formation and by acting as a diffusion barrier; gelatin will also affect the morphology of the reduction products. A similar switching was observed when gelatin was added to chloride electrolyte; surface analysis showed gelatin adsorption in this case. The black/white switching may, e.g. be useful for surfaces self-indicating corrosion potentials of galvanised steel.

1. Introduction

Zinc is an industrially important metallic coating material. Zinc and zinc-containing alloys are widely used on the million ton scale, amongst others for corrosion protection of steels, the most wide-spread structural materials. ZnO, the oxide of zinc, is a biocompatible, functional, semiconducting material with a wide direct bandgap of 3.3 eV [1, 2]. A large exciton binding energy makes ZnO suitable for a range of devices including catalysts, solar cells, sensors, photodetectors, laser and light-emitting diodes that operate in the blue and ultraviolet region of the spectrum [2]. For example, whispering gallery modes in spherical ZnO particles can be excited with visible light by coupling to defect-related transitions through free space [3]. In corrosion processes, ZnO can be grown with a rod-like morphology, which is suitable as a visible light photocatalyst [4]. The rod-like morphology obtained in the same corrosion processes shows in addition end-specific luminescence [5].

The surface of zinc is often further protected and functionalised by further coatings. Recent efforts lead to coating systems that respond to changes in the the electrode potential, given by the Fermi level of a metal

in contact with a liquid film or bulk electrolyte. During immersion of a metal in a solution, the electrode potential developing spontaneously on the metal is governed by the environment and the rates of the different possible redox reactions [6]. For example, the response of a polymer-based system to changes in corrosion potential after initiation of a corrosion process has been used to start a self-healing process in a sophisticated capsule based system [7, 8]. In corrosion protection in general, other triggers than the electrode potentials have been used, such as pH or laser illumination to trigger surface transformations, such as release or wettability transitions [9, 10].

Our group has recently investigated the possibility to use the biopolymer chitosan as ingredient in passive corrosion protection systems on zinc to limit ion mobility along the interface [11]. The cyclic oligosaccharide β-cyclodextrin was used to enhance corrosion inhibitor availability by incorporation into a model coating on zinc and into a zinc oxide based pretreatment [12, 13]. Aim of this work was to investigate the electrochemical properties of gelatin-modified zinc. Gelatin, a natural and water soluble protein, is an important functional ingredient in many food, pharmaceutical and cosmetic products owing to its adhesive, foaming, gelling, emulsifying and film forming properties [14, 15]. Gelatin remains one of the most important and widely used biopolymeric systems, as it is edible, biodegradable and non-toxic [16, 17]. It is also biocompatible in physiological environments, as well as water permeable, stimuli-responsive and inexpensive [18, 19]. It may be combined with other biopolymers in polyelectrolyte complexes, such as shown for polysaccharides carrageenan and chitosan [20].

In this work, gelatin films were prepared on oxide-covered zinc by two methods. The electrochemical behaviour of the surfaces was investigated in cyclic voltammetry (CV), an experiment with cyclic electrode potential variation. The resulting surfaces were characterised by scanning electron microscopy (SEM), Raman, infrared (IR) and x-ray photoelectron (XP) spectroscopy. The results will show an unusual switching of the optical appearance.

2. Experimental

2.1. Materials
Zinc sheets (purity 99.95%) were obtained from Goodfellow, Cambridge, UK. Samples (2 cm $\times$ 2 cm) were mechanically ground with 400, 1000, 2500 and 4000 grit SiC grinding paper. Metal pieces were ultrasonicated in ethanol, then rinsed with ultra-pure water and dried under a nitrogen stream. Gelatin was purchased from VWR Prolabo BDH Chemicals, Germany, and potassium chloride from J.T. Baker. All reagents were used without further purification.
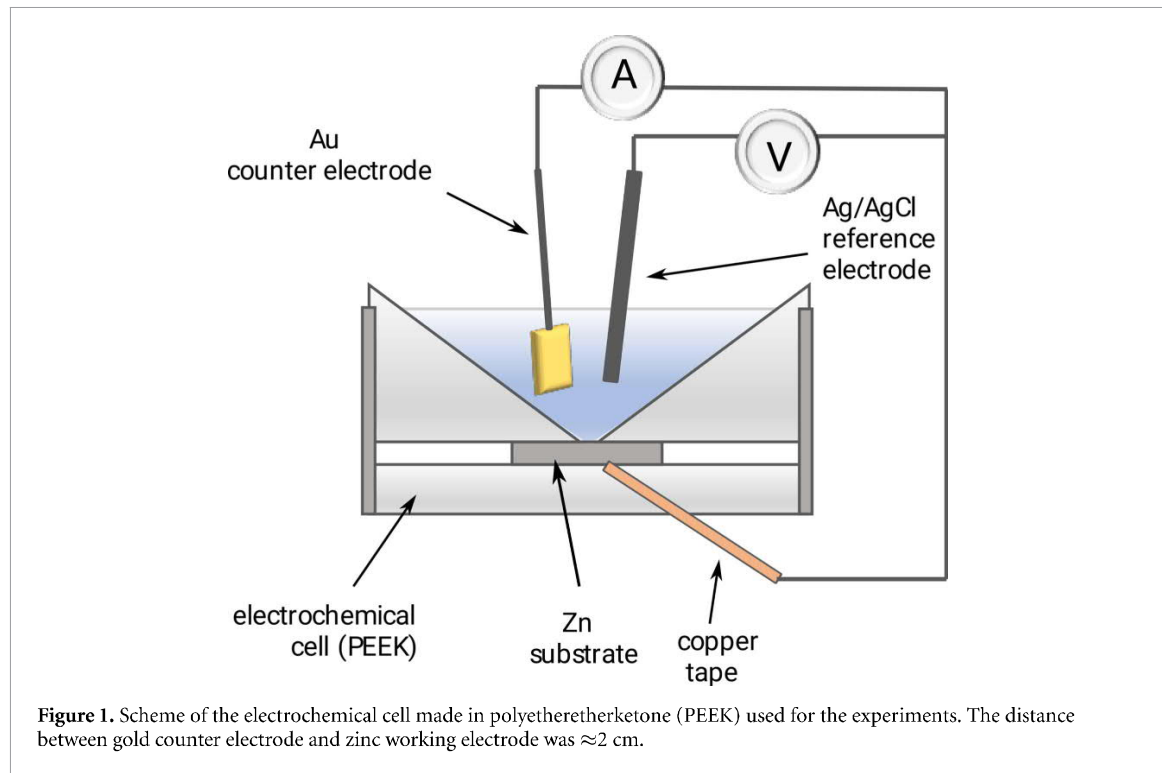
2.2. Film preparation
Gelatin solutions were prepared in 3% (weight per volume) and 2% (weight per volume) concentration, by adding 3 g or 2 g of gelatin powder to 100 ml of ultrapure water, respectively. Each solution was stirred vigorously at first, then mixing was continued in an oil bath at 45 °C for 5 h to enable complete dissolution of the gelatin. Finally, the solutions were purged with argon, stored in a sealed container refrigerated at 4 °C and protected from light.

In the first approach, zinc samples were coated with 3% gelatin solution via the doctor blading method using a 24 μm spiral doctor blade, dried under air stream at 90 °C and subsequently thermally cured at 100–105 °C for 2 h in an oven in vacuum to remove residual water from the coating. The second sample preparation method involved gelatin as a part of the electrolyte in an electrodeposition system. A mixture of solutions was used, consisting of 2% gelatin and 0.1 M KCl in a volume ratio 1:1.

Additionally, borate buffer was prepared for control experiments. The buffer consisted of 2.2 mM $Na_2B_4O_7 \cdot H_2O$. Its pH was adjusted to 9.3 $\pm$ 0.2 by addition of NaOH up to a concentration of 2.2 mM.

2.3. Electrochemical treatment
Either a coated, or a bare zinc substrate acted as a working electrode of a three electrode setup in a home-made electrochemical cell (figure 1) set on top of the zinc sheet. At the bottom of the conical electrolyte volume, a circular area with a radius of $\approx$0.75 cm was in contact with the electrolyte. The cell contained a gold foil as a counter electrode and a commercial Ag/AgCl (3 M KCl) reference electrode (Metrohm, Filderstadt, Germany). All electrode potentials in this work are referred to Ag/AgCl (3 M KCl). The electrolyte was either 0.1 M KCl (pH 7.0 $\pm$ 0.1) only, or a mix of 0.1 M KCl and gelatin, as specified before. An Ivium Technologies Iviumstat potentiostat was used to record CVs. All measurements shown here were carried out at a scan rate of 10 mV s^{-1}. Current values obtained from CV experiments were area normalized to the zinc surface area of 1.77 cm^2 in contact with the electrolyte. Measurements were designed to initiate sample polarisation from close to the open circuit potential (OCP), which for all samples was

Figure 1. Scheme of the electrochemical cell made in polyetheretherketone (PEEK) used for the experiments. The distance between gold counter electrode and zinc working electrode was ≈2 cm.

around −1 V. Samples were first polarised in the negative direction. Prior to each measurement, the system was equilibrated at the starting potential for 2 s.

2.4. Characterisation methods

A consumer digital camera was used to record sample pictures and the video of the switching.

For surface characterisation, IR spectra were obtained using a Bruker Vertex 70v FTIR spectrometer equipped with a nitrogen cooled middle band mercury cadmium telluride (MCT) detector. Spectra were recorded with a spectral resolution of 4 cm^{-1} in external reflection geometry at an angle of incidence of 80° using p-polarised light, accumulating 250 scans. Bare zinc served as a reference for each measurement.

X-ray photoelectron (XP) spectra were used to gather evidence of chemical structure alteration of the gelatin films after electrochemical treatment. XPS measurements were carried out with a Physical Electronics Quantera 2 spectrometer employing an Al Kα source (1 486.6 eV) at a pass energy of 26 eV and with energy step of 0.1 eV. The take-off angle was 45°. The binding energy scale was referenced to the C–C signal at a binding energy of 284.8 eV.

A Zeiss 1550 VP Field Emission SEM was used to obtain information on sample's morphology.

On a commercial confocal Raman microscope (Witec), a 50× magnification long working distance microscope objective was employed to select a point to focus the laser beam spot on the sample surface. A 532 nm laser source was utilised, with 50 mW laser power, 2 s integration time and 15 accumulations for each point measurement.

Characterisation results presented were obtained after 3 complete CV cycles when referred to as "after CV", and on the reverse scan of the first anodic or second cathodic cycle when referred to as "white" or "black", respectively.

3. Results and discussion

3.1. Electrochemical treatment of gelatin

Three different sample sets were used, namely a bare zinc control, gelatin-coated zinc and bare zinc in electrolyte containing both gelatin and KCl. Potential scans were initiated in the negative direction from around the OCP, ≈−1.0 V. The scan direction was reversed at −1.5 V and the scan proceeded in the positive direction until −0.5 V (figure 2(a)). The voltammogram recorded shows a sharp increase in anodic current, which starts in the reverse scan at around −1.0 V. When the potential is cycled between −1.5 and −0.5 V, the first cycle differs notably from the other two. Figure 2(b) shows two reduction and two oxidation processes in the first cycle. They are labelled as C₁ and C₍₂₎ in the cathodic scan, and A₁ and A₂ in the anodic scan. In the
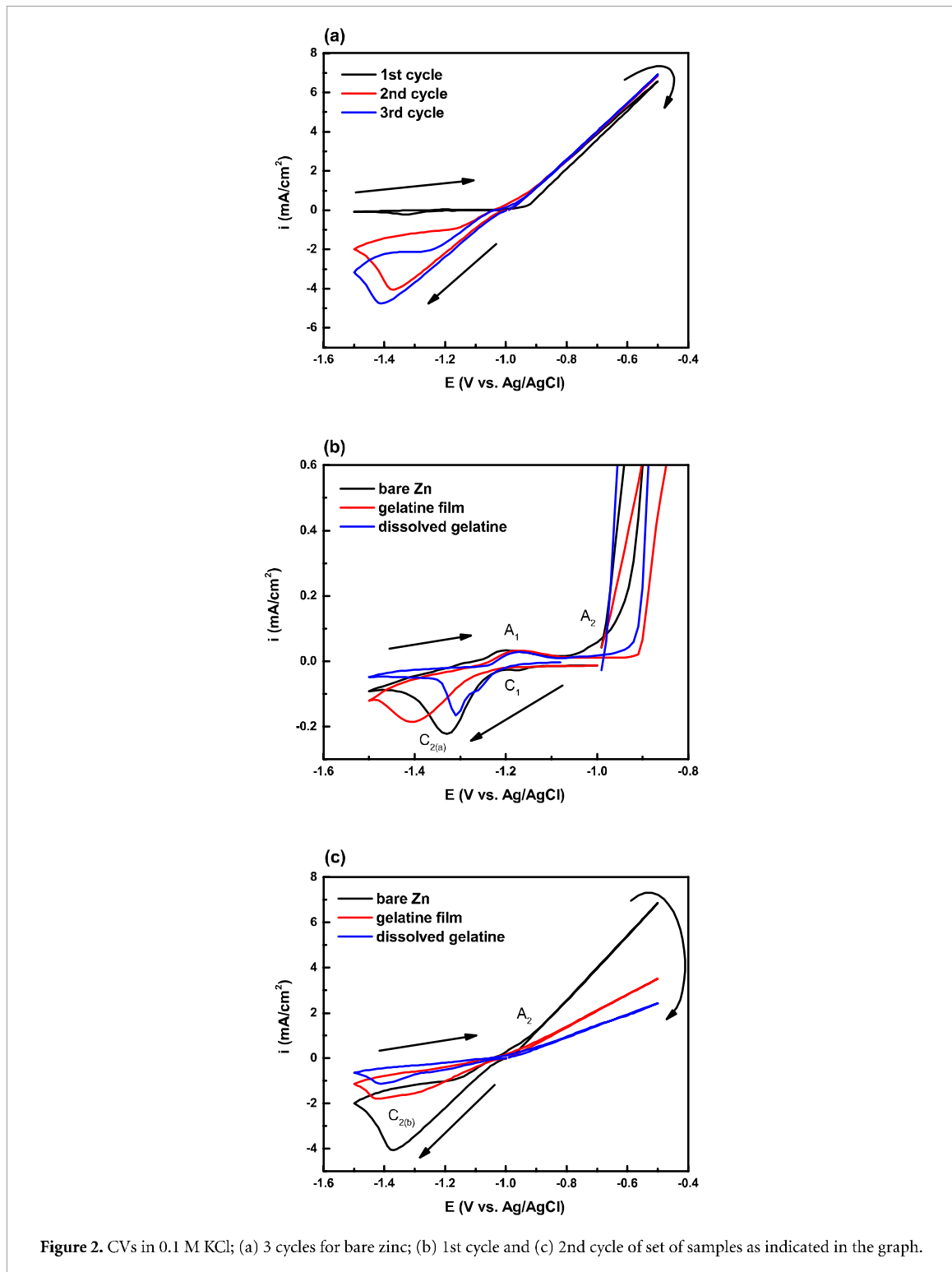
Figure 2. CVs in 0.1 M KCl; (a) 3 cycles for bare zinc; (b) 1st cycle and (c) 2nd cycle of set of samples as indicated in the graph.

second cycle (figure 2(c)), peaks A_1 and C_1 disappear and peak $C_{2(b)}$ develops at a similar potential as $C_{2(a)}$, however with a much higher cathodic current.

CVs in the same potential range on samples with gelatin film or dissolved gelatin results in very similar voltammogram shapes in first and consecutive cycles (figure 2(a) and (b)). Comparing the first cycle in the presence and absence of gelatin (figure 2(b)), the current densities of the anodic A_1 as well as the cathodic $C_{2(a)}$ peaks are shifted. Both current densities decrease in the presence of gelatin. In the case of gelatin-coated zinc the anodic peak A_1 is shifted towards more positive potentials, whereas the $C_{2(a)}$ cathodic peak is shifted toward more negative potentials in relation to bare zinc. Control experiments show gelatin-covered zinc to remain passive in borate buffer, with a lower peak current intensity than usual for zinc in borate. In the comparison of the second cycle of different samples, a big difference in the current density range is observed
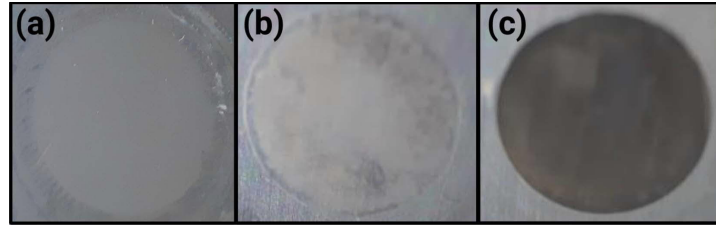
Figure 3. Visible images of gelatin-covered zinc after CVs in 0.1M KCl, where the CV was interrupted at different stages; (a) after the first cathodic half-cycle; (b) after the first anodic scan up to 0.7 V vs. Ag/AgCl (3M KCl) (c) after the second cathodic scan at −1.2 V vs. Ag/AgCl (3M KCl).
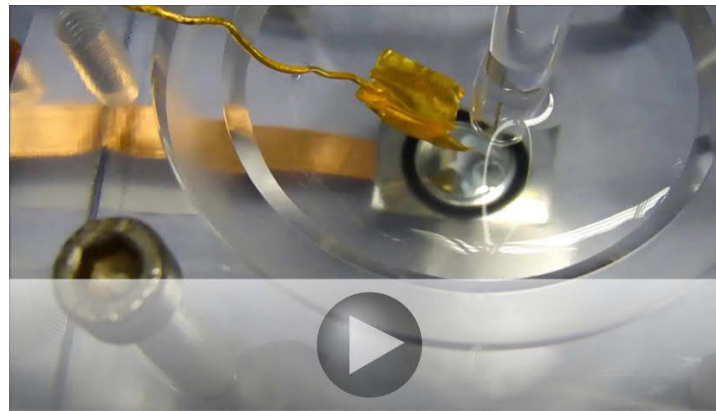

Figure 4. Switching of surface appearance in the electrochemical cell.

in the presence and absence of gelatin (figure 2(c)). The shape of the cathodic peak $C_2(b)$ in gelatin resembles the one for bare zinc. However, the current density decreases to less than half when gelatin coating is measured, and even more when dissolved gelatin is utilised as the electrolyte. Obviously, both the gelatin coating before CV as well as the adsorption of gelatin to the substrate inhibit charge transfer between the metal and the solution.

3.2. Characterisation of surfaces

Figure 3 shows images of zinc covered with a gelatin-film indicating the optical appearance in the different potential regimes. During the first cathodic sweep, the surfaces remains metallic and becomes a little darker (figure 3(a)). In the first anodic scan, the surface becomes whitish during peak A_2 (figure 3(b)). In the second cathodic scan, the surface becomes black (figure 3(c)) when passing through current peak $C_2(b)$. During subsequent cycles, the surface appearance changes between a white state associated with anodic currents above the OCP and a black state associated with the cathodic current peak below the OCP. The switching between the two states is shown in figure 4. The maximum number of cycles one can switch before the surface properties fade has not been investigated systematically here. Control samples in the absence of gelatin showed no switching. During the first cathodic scan, the samples in the absence of gelatin darkened similar to what is shown in (figure 3(a)) and remained in this state during subsequent cycling.

SEM images on electrochemically treated zinc (figure 5(a) and (b)) show characteristic zinc corrosion products in a form of hexagonal structures as well as the presence of pits on the surface. It was previously found that the hexagonal plates consist mostly of metallic zinc as well as ZnO [21–23]. After electrochemical treatment, randomly distributed pits and pits forming straight lines were observed for both coating methods (figure 5). Comparing the images of gelatin-covered zinc before and after CV (figure 5(c) and (d), respectively) suggests that a significant amount of gelatin redissolves during CVs.

Raman spectra of the zinc sample (figure 6) exhibit a broad peak at ≈ 560 cm^{-1}. When magnified, the peak can be separated into independent components at ≈ 350, ≈ 440 and ≈ 560 cm^{-1}. These are characteristic for ZnO [24, 25], and are present in all samples after CVs. The peak at ≈ 560 cm^{-1} is assigned to longitudinal optical (LO) phonon of ZnO (E_1 and A_1 modes), 440 cm^{-1} to E_2 (high) mode of the hexagonal wurtzite lattice of ZnO and 350 cm^{-1} to A_1 mode (TO phonon) [23–26]. Dominance of the LO phonon is typical for defect-rich ZnO, amongst others generated in electrochemical processes [5, 23, 27].
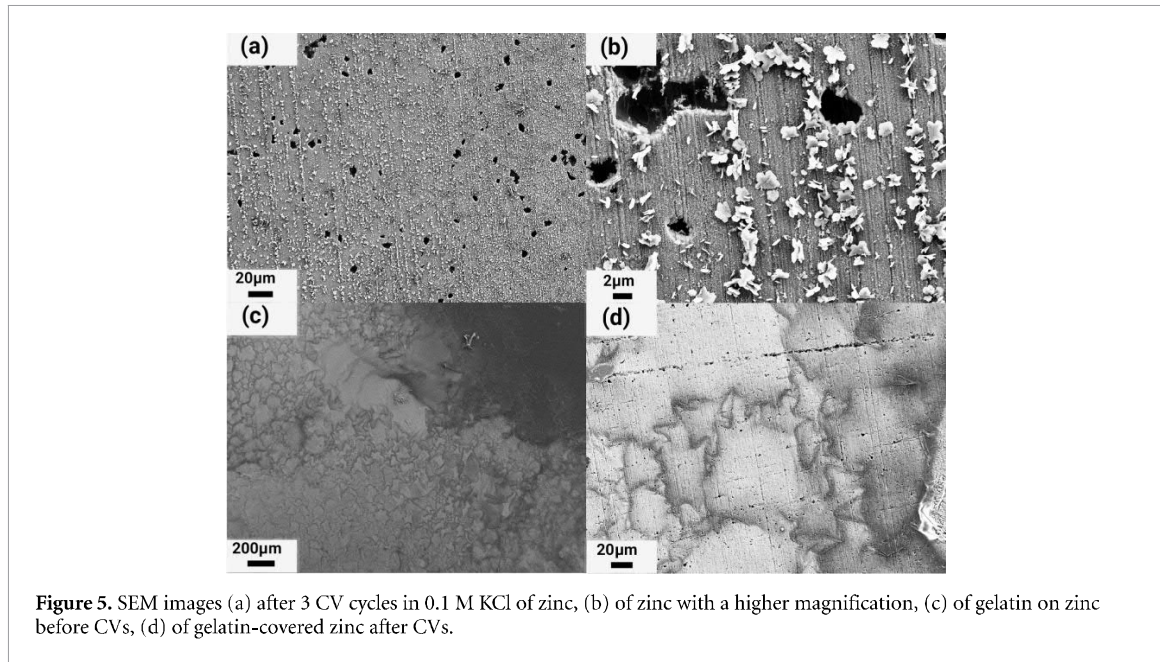
Figure 5. SEM images (a) after 3 CV cycles in 0.1 M KCl of zinc, (b) of zinc with a higher magnification, (c) of gelatin on zinc before CVs, (d) of gelatin-covered zinc after CVs.
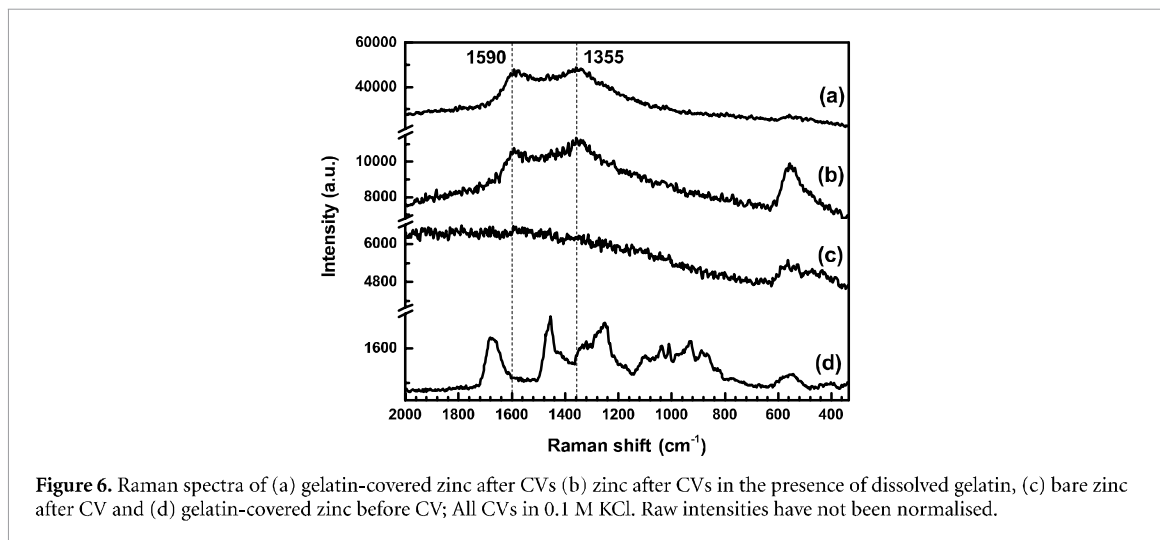

Figure 6. Raman spectra of (a) gelatin-covered zinc after CVs (b) zinc after CVs in the presence of dissolved gelatin, (c) bare zinc after CV and (d) gelatin-covered zinc before CV; All CVs in 0.1 M KCl. Raw intensities have not been normalised.

The spectra recorded of gelatin-coated zinc samples before CVs show the typical spectrum of gelatin [28]. In control experiments in borate buffer, spectra of gelatin-covered zinc after CVs also show the same gelatin peaks. On the other hand, Raman spectra of gelatin-covered zinc after CVs in chloride (figure 6(a)) feature three distinctive peaks. The ZnO feature at 560 cm^{-1} is detected, as well as two well separated peaks at 1355 and 1590 cm^{-1}. Peaks around 1570–1590 cm^{-1} correspond to the G band and are related to sp^2 carbon microdomains, characteristic for graphite-like materials [29–31]. The D band peaks around 1345–1355 cm^{-1} are associated with bond-angle disorder in the sp^2 graphite-like domains, induced by linking with sp^3 carbon atoms as well as by the finite crystalline sizes of sp^2 microdomains [30, 31]. The absence of a G' peak in formed carbon indicates its amorphous nature [32].

It is also worthwhile to analyse the level of the luminescence background in the Raman spectra in figure 6. In the untreated, gelatin coated samples, this background is lowest. The luminescent background on the bare zinc sample after CVs is already ≈5 times higher; strong defect related luminescence is commonly observed in oxide on zinc [5, 23]. Compared to the initial state, gelatin-covered zinc surfaces show an increase in luminescence background by 1 1/2 orders of magnitude. Such strong luminescence would hide peaks of gelatin with the intensity as observed before CVs. Luminescence is also an indication of light absorption in the films, consistent with the black appearance. Conversion of carbon-source material into graphitic carbon and DLC upon laser excitation has been reported [33, 34], and is commonly observed during Raman spectroscopy. On the other hand, experiments with the chosen illumination geometry before CV application show clearly a gelatin spectrum. Formation of the carbon structures must thus be a consequence of the electrochemical modification of the thin film; we consider it likely that the strong light
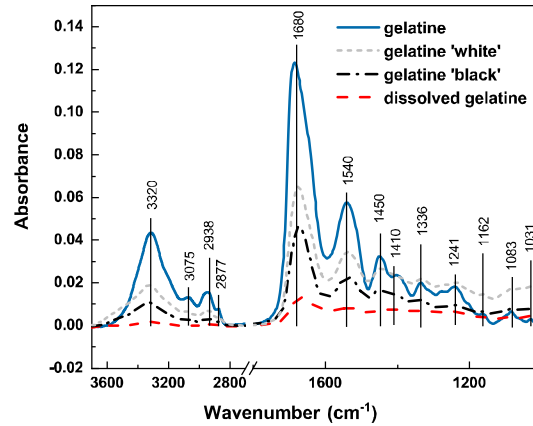
Figure 7. IR spectra of gelatin coated zinc before and after different stages of electrochemical treatment in 0.1M KCl. The background was a blank zinc sample.

absorption on the black surfaces triggers chemical transformation of the organic species into carbon during Raman experiments. The latter is not unexpected, as rather high illumination intensities were needed in order to obtain high quality spectra. Crystalline carbon by itself is also not expected to show luminescence.

Figure 7 shows IR spectra of the gelatin film before and after electrochemical treatment and a spectrum of the zinc surface after CV in dissolved gelatin. The spectra show characteristic peaks for gelatin. The typical peaks and their assignment are available in the literature [28, 35]. IR results provide evidence that after conducting CVs on gelatin coated zinc, the polymer is still present on the surface. Nevertheless, the absorbance decreases to less than a half after electrochemical treatment in KCl, and the main decrease already happened at the end of the first cycle. No structural differences are obvious between the surface in the black and in the white state. The presence of characteristic polymer peaks indicates that deposition of gelatin took place after cyclic polarisation of zinc in KCl solution containing dissolved gelatin, in line with electrochemical results.

The main peak in the amide region, typically the amide I mode, was observed here initially at 1685 cm^{-1}, thus at substantially higher wavenumber than typically obtained for fully hydrated gelatin in the literature [35–38]. Even in highly concentrated solutions [39], the amide I mode is in the region 1650–1660 cm^{-1}. The observed high wavenumber may be caused by a high fraction of β-turns or partially dehydrated structures, but given the preparation method, the latter is more likely [37, 38]. After the CVs, the amide I peak is shifted to $\approx$1670 cm^{-1}, thus closer to the typically observed value, indicating rehydration of the gelatin [35–38, 40]. There is no significant change in the shape of the spectra in the amide region, as would be expected e.g. for the formation of molecular aggregates. Additionally, peaks around 1200–800 cm^{-1} change in absorbance. However, neither do new peaks appear above baseline level, nor do peaks disappear. Some changes are, however, difficult to interpret in detail.

XP spectra of gelatin-coated samples before and after different stages of electrochemical treatment are shown in figure 8. The C 1s spectra of the films before and after electrochemical treatment are compared, each fitted with three distinct peaks at 288.0, 286.1 and 284.8 eV, corresponding to O-C = O/N-C = O, C-O/C-N and C-C/C-H, respectively [18, 41]. The O 1s spectrum is fitted with two components corresponding to C-O and Zn(OH)$_2$ at $\approx$532.5 eV and C = O/ZnO at $\approx$531.3 eV [23, 42–44]. A further disambiguation of organic and inorganic oxygen would be an overinterpretation of the data. The small differences between the region before and after electrochemical treatment in relation the relatively large differences in the C 1s peak points to a domination of inorganic species in the O 1s region. The N 1s signal needs to be fitted with two peaks at 399.7 and 398.1 eV, corresponding to C-N/C = N and nitride/Zn-N, respectively [18, 45]. The latter represents only a minor component. The visibility of the Zn 2p peaks shows that the organic gelatin layer is not completely covering the zinc. The C 1s and N 1s regions of XP spectra show characteristic peaks corresponding to polypeptides and proteins. The C 1s region reveals an increase of oxygen bound carbon after electrochemical treatment, with only minor differences between black and white samples. Electrochemical treatment of gelatin induced a significant increase in the fraction of oxygen-bound carbon. Treatment also increased the Zn 2p intensities relative to the C 1s peak, confirming that some organic material covering the zinc was lost. Overall, differences between spectra from samples emersed after treatment to different potentials are rather small, indicating only minor differences in elemental composition. The small differences also indicate that the predominant part of the oxidation of the gelatin layer takes place during the initial stages of the experiment.
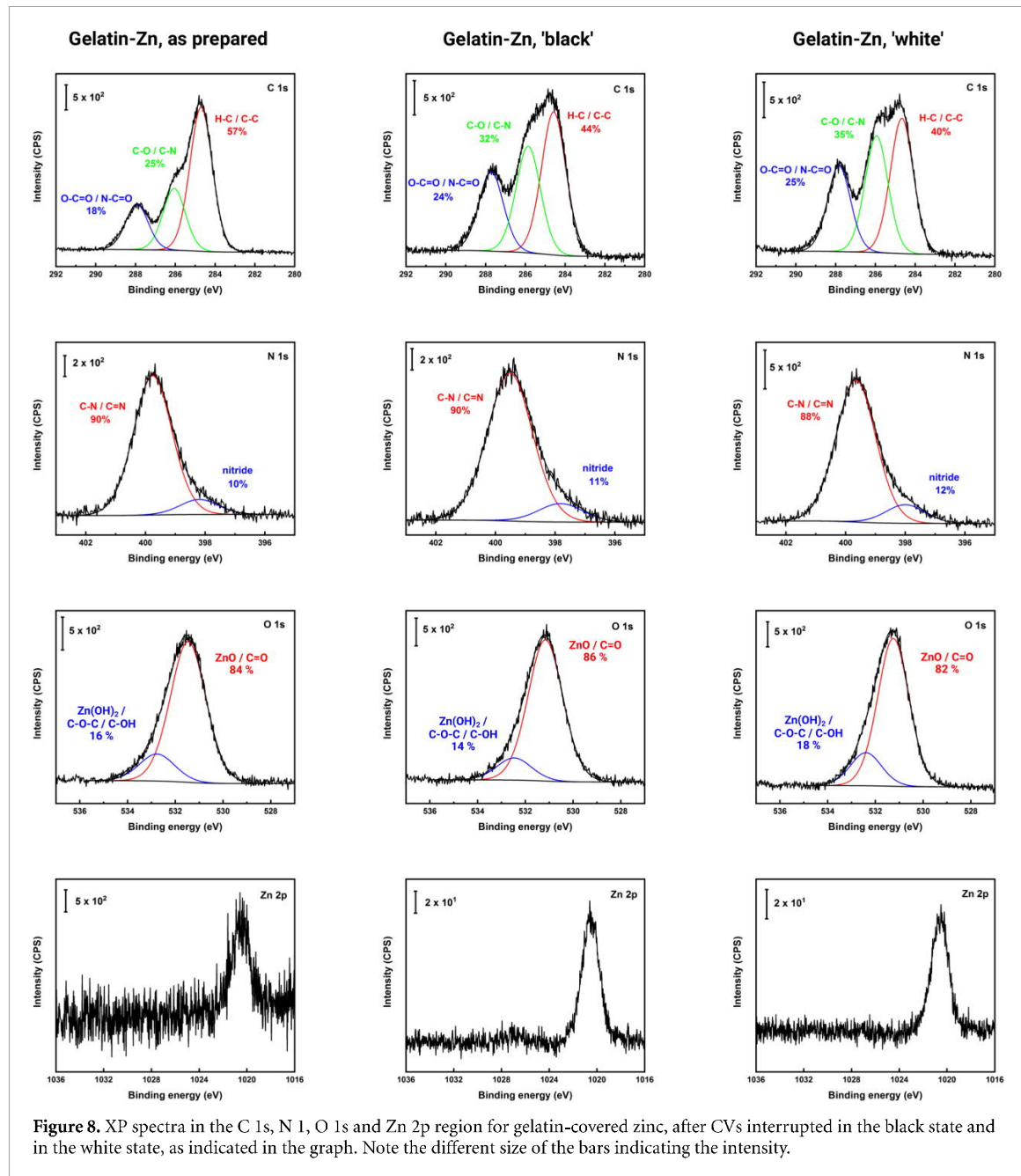
Figure 8. XP spectra in the C 1s, N 1, O 1s and Zn 2p region for gelatin-covered zinc, after CVs interrupted in the black state and in the white state, as indicated in the graph. Note the different size of the bars indicating the intensity.

3.3. Discussion of surface structure of obtained films and switching mechanism

The prepared surfaces behave as a 'smart', stimuli-responsive system. In general, such systems offer interesting opportunities. For example, they enable flexible diffraction gratings [46]. In polymeric systems, stimuli responsive polymeric systems are of great interest in biomedical applications [47]. Stimuli-responsive interfaces are thus a very active field of research. On a more general level, electrode potential response was, amongst others, found to mediate cell surface interactions and cell development [48].

The SEM micrographs recorded after CVs (figure 5(a) and (b)) show, amongst others, pits as a result of pitting corrosion. A sharp increase in current density as observed in the electrochemical experiments (figure 2) is also characteristic for pitting corrosion on otherwise oxide-passivated metals in media containing complexing ions such as chloride anions [19, 49, 50]. The C_1 and $C_{2(a)}$ peaks in figure 2(b) are attributed to reduction of Zn^{II} to metallic zinc. The anodic peak A_1 is characteristic for dissolution and formation of $Zn(OH)_2$ and ZnO [51, 52]. In chloride containing systems, a multilayer structure of the generated film could be present due to coexistence of a number of different species such as Zn^{2+}, $ZnCl^+$, $Zn(OH)^+$, $Zn_5OH_8Cl_2$, $(ZnCl_4)^{2-}$, $ZnCl_2$, $Zn(OH)_2$ and ZnO [53–55].

When the electrode is scanned to sufficiently high electrode potential, a sharp increase in current occurs, labelled A_2 (figure 2(b)). A_2 is attributed to a metal dissolution current. The observed peak shifts indicate that the gelatin film creates a kinetic barrier for zinc redox reactions on the surface. Moreover, in the case of
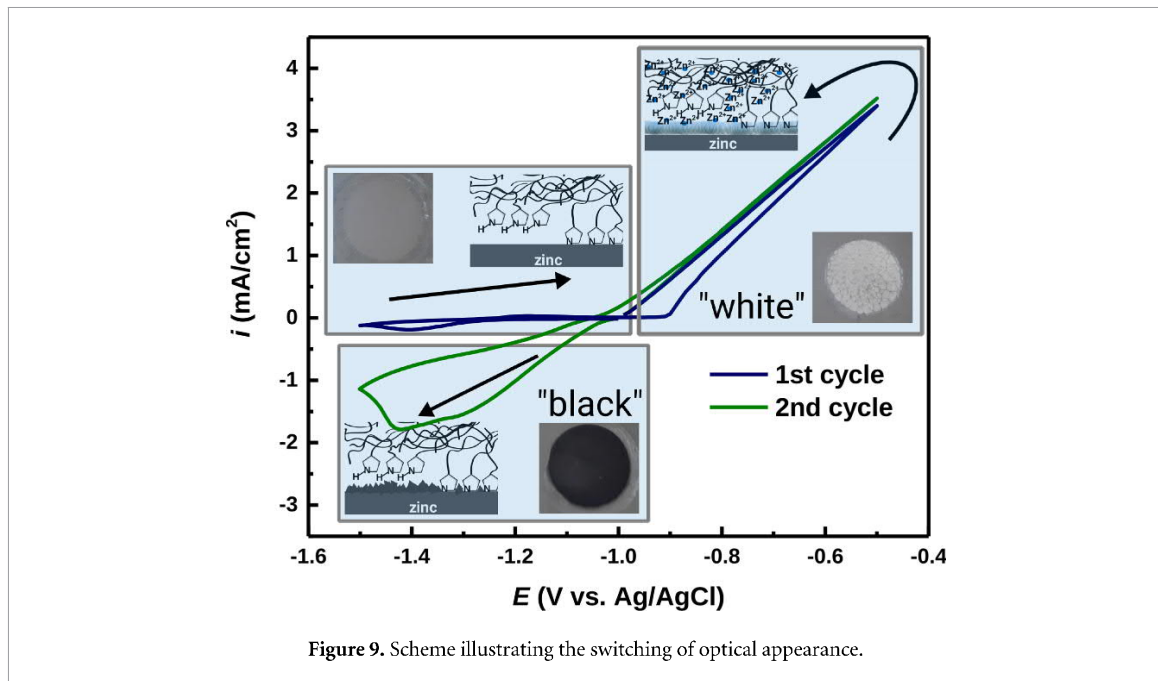
Figure 9. Scheme illustrating the switching of optical appearance.

dissolved gelatin, the shift of the anodic peak towards more positive potentials implies that gelatin is inhibiting the oxidation reaction of the substrate. However, the cathodic peak is also shifted in the same direction. Suppression of reduction reaction by dissolved gelatin is indicated by a decrease in current density. Peaks C_1 and $C_{2(a)}$ are brought closer together than in the case of the bare metal substrate. When the CV is run in a dissolved gelatin system, the C_1 peak is still present due to the lack of a pre-deposited gelatin film on the substrate. In this case, when metal is not coated, the current of zinc related reactions in the first cycle increases. In both samples containing gelatin, the onset of pitting is shifted towards more positive potentials.

Overall, the decrease of current densities in the dissolved gelatin system in comparison with the gelatin films originates from continuous supply of gelatin molecules to the substrate. As a result, the suppression of redox reactions by gelatin on metallic zinc is more pronounced. On the other hand, the gelatin-containing electrolyte has a lower conductivity, potentially inducing larger Ohmic potential drop in the system and causing a difference in CV curves.

The results of the surface analysis show that ZnO is forming on the surface during the anodic parts of the CVs. The white appearance during this part of the CV is thus easily attributed to the formation of a white ZnO layer. SEM shows in some regions the substrate underneath that layer, and while electrochemically, the system behaves passive in borate buffer, no passivation is observed in chloride containing electrolytes. Thus, the presence of gelatin has no part in the induction of pitting and zinc dissolution.

During the cathodic peak $C_{2(b)}$, which is first observed in the second CV cycle and is present afterwards, reduction of ZnO and Zn^{2+} formed in the first anodic cycle occur at the same time as the surface appearance changes from white to dark, brown-black. For simplicity, the latter will be referred to as 'black'. Two possible reasons shall be discussed here for the observed darkening, (i) the oxidation and reduction of zinc species and (ii) the formation of carbon from gelatin.

Our group and others have in the past discussed that zinc surfaces can appear dark after electrochemical reduction [23, 56], or after formation of defect-rich thick ZnO layers [4, 5, 57–59]. An oxidation of zinc with a subsequent reduction of dissolved species near the metal surface is also fully consistent with the electrochemical data obtained. ZnO is clearly detected in the Raman spectra.

On the other hand, the organic gelatin may transform into carbon during electrochemical treatment. Indeed, carbon nanostructures can be synthesised e.g. in anodised aluminium templates [60]. Raman spectra suggest at first glance carbon formation, however, analysing the background fluorescence which should be absent for a material without band gap, the IR, and the XPS, leads us to conclude that carbon formation occurs during the Raman experiment which had to be conducted with rather high intensity in order to be sufficiently sensitive. This transformation may be caused only after electrochemical treatment because of increased light absorption and consequent increased local heating at the black surfaces, or because electrochemical treatment induced damages in the gelatin structure. IR spectra are consistent with a decrease in the amount of gelatin on the surface, while XPS shows an increase in the fraction of oxidised C-atoms compared to aliphatic and aromatic C-atoms. Taken together, IR and XPS thus point to a loss in aliphatic and aromatic carbon in gelatin during cycling. The observed IR spectra are also not consistent with the formation

of an oxidised aromatic C-system as dominating species: in that case, the $C = O$ stretching modes are supposed to shift to wavenumbers >1700 cm^{-1}, but a shift to lower wavenumber is observed. While surface analysis leaves the possibility that carbon forms at the polymer/metal interface where it is not detected by XPS and only affects the background in the IR, the electrochemical properties of the black, reduced surfaces are still those of zinc. In particular, there is no reason to assume that carbon-based materials would be oxidised at the same potential as zinc. On the contrary, some carbon-nitrogen containing material has been shown to be quite stable towards oxidation [61, 62].

We thus reason that the reversible switching between a white surface at high potentials and a black surface at low potentials is caused by the zinc electrochemistry in the gelatin film, as illustrated in figure 9. During oxidation, ZnO and Zn^{2+} form. As opposed to the situation for bare zinc surfaces, Zn^{2+} is trapped inside the gelatin layer near the surface. Subsequent reduction will thus generate a zinc surface with a morphology of the metal/polymer interface which facilitates light absorption after multiple scattering. During the next oxidation cycle, the formed zinc species will be oxidised again. It is important to realise that the surfaces will never be completely oxide free, but the reduced oxide is also typically dark [56].

As to the retention of Zn^{2+} inside the gelatin layer, zinc-amino acid complexation is often encountered [63]. It is a popular way to increase bioavailability and absorption of zinc in dietary supplements [64]. It was shown that components of gelatin like hydroxyproline and hydroxylysine, which are not as frequently used amino acids chelates, may also complex zinc [65]. Moreover, reversible zinc complexation has also been described [66, 67]. Thus, some sort of complexation of Zn^{2+} in the gelatin layer on zinc is expected. Both ex situ XP and IR spectra obtained here show that there is only a small difference in composition between black and white surfaces in this work, supporting the argument that the main difference is related to formation and reduction of Zn^{2+}. Preadsorbed gelatin is significantly altered in the first cycle, but SEM, XPS and IR indicate smaller changes in the later stages of the experiment. The limits of stability have not been investigated systematically. Gelatin is adsorbed to zinc and would thus naturally affect the morphology of the formed zinc electrodeposit during reduction.

It is worth noting that the observed phenomenon is qualitatively different from electrochromism, where a specific absorption colour of a film of a certain substance is switched electrically [68, 69]. In the case reported in this paper, the scattering of light is tuned by the surface properties.

4. Conclusions

The optical appearance of zinc can be reversibly switched electrochemically after coating zinc with gelatin between a black surface below the OCP and a white surface above the OCP in chloride-containing electrolyte. A similar switching is observed after adding dissolved gelatin to chloride-containing electrolyte. The gelatin backbone remains largely intact during the cycling, though some damage of the film does occur, especially during the first cycle. Surface analysis shows only minor chemical differences in the gelatin component of the layer when comparing the black and the white surfaces. The white appearance at more positive potentials is caused by the formation of zinc oxide. The black appearance at the lower potentials is likely originating from light absorption in reduced defect-rich zinc oxide and the morphology of redeposited metallic zinc. The function of the gelatin layer is to retain zinc ions that form during the pitting corrosion process near the zinc surface, i.e. to prevent transport into the bulk solution. These ions would therefore be available for subsequent reduction. A further role of gelatin is presumably to control the morphology during zinc redeposition. Addition of gelatin to the electrolyte yields an adsorbed gelatin layer *in situ*, whereas pre-adsorption yields a better defined layer at the beginning. The demonstrated switching principle could be used to switch appearances of metallic surfaces at the large scale e.g. on galvanised steel. Gelatin coating may on the other hand also serve to realise self-indicating surfaces where the onset of a corrosion process, accompanied by a change in OCP, leads to a change optical appearance of the surface.

ORCID iDs

Agnieszka Natalia Ksiazkiewicz https://orcid.org/0000-0002-9024-3588
Andreas Erbe https://orcid.org/0000-0002-7988-1538

References

[1] Sirelkhatim A, Mahmud S, Seeni A, Kaus N H M, Ann L C, Bakhori S K M, Hasan H and Mohamad D 2015 Review on zinc oxide nanoparticles: antibacterial activity and toxicity mechanism *Nano-Micro Lett.* **7** 219–42

[2] Kolodziejczak-Radzimska A and Jesionowski T 2014 Zinc oxide—from synthesis to application: a review *Materials* **7** 2833–81

[3] Moirangthem R S and Erbe A 2013 Interfacial refractive index sensing using visible-excited intrinsic zinc oxide photoluminescence coupled to whispering gallery modes *Appl. Phys. Lett.* **103** 051108

[4] Iqbal D, Kostka A, Bashir A, Sarfraz A, Chen Y, Wieck A D and Erbe A 2014 Sequential growth of zinc oxide nanorod arrays at room temperature via a corrosion process: application in visible light photocatalysis *ACS Appl. Mater. Interfaces* **6** 18728–34

[5] Iqbal D, Sarfraz A and Erbe A 2018 Gradient in defect density of ZnO nanorods grown by cathodic delamination, a corrosion process, leads to end-specific luminescence *Nanoscale Horiz.* **3** 58–65

[6] Frankel G, Landolt D 2007 Fundamentals of corrosion - kinetics of electrolytic corrosion reactions *Encyclopedia of Electrochemistry* vol 4 ed A Bard, M Stratmann and G Frankel (Weinheim Germany: Wiley) Ch 1 1–60

[7] Vimalanandan A, Lv L P, Tran T H, Landfester K, Crespy D and Rohwerder M 2013 Redox-responsive self-healing for corrosion protection *Adv. Mater.* 6980–6984

[8] Tran T H, Vimalanandan A, Genchev G, Fickert J, Landfester K, Crespy D and Rohwerder M 2015 Regenerative nano-hybrid coating tailored for autonomous corrosion protection *Adv. Mater.* **27** 3825–30

[9] Wang T, Du J, Ye S, Tan L and Fu J 2019 Triple-stimuli-responsive smart nanocontainers enhanced self-healing anticorrosion coatings for protection of aluminum alloy *ACS Appl. Mater. Interfaces* **11** 4425–38

[10] Yong J, Singh S C, Zhan Z, Chen F and Guo C 2019 Substrate-independent, fast, and reversible switching between underwater superaerophobicity and aerophilicity on the femtosecond laser-induced superhydrophobic surfaces for selectively repelling or capturing bubbles in water *ACS Appl. Mater. Interfaces* **11** 8667–75

[11] Fernández-Solis C and Erbe A 2016 Waterborne chitosan-epoxysilane hybrid pretreatments for corrosion protection of zinc *Biointerphases* **11** 021001

[12] Altin A, Rohwerder M and Erbe A 2017 Cyclodextrins as carriers for organic corrosion inhibitors in organic coatings *J. Electrochem. Soc.* **164** C128–C134

[13] Altin A, Vimalanandan A, Sarfraz A, Rohwerder M and Erbe A 2019 Pretreatment with a β-cyclodextrin - corrosion inhibitor complex stops an initiated corrosion process on zinc *Langmuir* **35** 70–7

[14] Nezhadi S H, Choong P F, Lotfipour F and Dass C R 2009 Gelatin-based delivery systems for cancer gene therapy *J. Drug Targeting* **17** 731–8

[15] Brodsky B, Werkmeister J A and Ramshaw J A M 2005 chap Collagens and Gelatins and *Biopolymers Online* ed A Steinbüchel (Weinheim, Germany: Wiley-VCH) DOI:10.1002/3527600035.bpol8006

[16] Mariod A A and Fadul H 2013 Review: gelatin, source, extraction and industrial applications *Acta Sci. Pol. Technol. Aliment.* **12** 135–47 https://www.food.actapol.net/volume12/issue2/abstract-1.html and https://www.food.actapol.net/volume12/issue/1_2_2013.pdf

[17] Gómez-Guillén M, Giménez B, López-Caballero M and Montero M 2011 Functional and bioactive properties of collagen and gelatin from alternative sources: A review *Food Hydrocolloids* **25** 1813–27

[18] Peng X, Liu Y, Bentley W E and Payne G F 2016 Electrochemical fabrication of functional gelatin-based bioelectronic interface *Biomacromolecules* **17** 558–63

[19] El Rehim S A, Fouad E, ElWahab S A and Hassan H H 1996 Electroplating of zinc-nickel binary alloys from acetate baths *Electrochim. Acta* **41** 1413–18

[20] Al-Zebari N, Best S M and Cameron R E 2018 Effects of reaction pH on self-crosslinked chitosan-carrageenan polyelectrolyte complex gels and sponges *J. Phys. Mater.* **2** 015003

[21] Xu F, Yuan Z Y, Du G H, Halasa M and Su B L 2007 High-yield synthesis of single-crystalline ZnO hexagonal nanoplates and accounts of their optical and photocatalytic properties *Appl. Phys. A* **86** 181–5

[22] Kumari L and Li W 2010 Synthesis, structure and optical properties of zinc oxide hexagonal microprisms *Cryst. Res. Technol.* **45** 311–15

[23] Chen Y, Schneider P, Liu B J, Borodin S, Ren B and Erbe A 2013 Electronic structure and morphology of dark oxides on zinc generated by electrochemical treatment *Phys. Chem. Chem. Phys.* **15** 9812–22

[24] Sander T, Eisermann S, Meyer B K and Klar P J 2012 Raman tensor elements of wurtzite ZnO *Phys. Rev. B* **85** 165208

[25] Özgür U, Alivov Y I, Liu C, Teke A, Reshchikov M, Doğan S, Avrutin V, Cho S J and Morkoc H 2005 A comprehensive review of ZnO materials and devices *J. Appl. Phys.* **98** 041301

[26] Cuscó R, Alarcón-Lladó E, Ibanez J, Artús L, Jiménez J, Wang B and Callahan M J 2007 Temperature dependence of Raman scattering in ZnO *Phys. Rev. B* **75** 165202

[27] Tay Y Y, Tan T T, Liang M H, Boey F and Li S 2008 Nature of quasi-LO phonon in ZnO *Appl. Phys. Lett.* **93** 111903

[28] Meade A D, Lyng F M, Knief P and Byrne H J 2007 Growth substrate induced functional changes elucidated by FTIR and Raman spectroscopy in in-vitro cultured human keratinocytes *Anal. Bioanal. Chem.* **387** 1717–28

[29] Ferrari A C and Robertson J 2004 Raman spectroscopy of amorphous, nanostructured, diamond-like carbon, and nanodiamond *Philos. Trans. R. Soc. A* **362** 2477–2512

[30] Chu P K and Li L 2006 Characterization of amorphous and nanocrystalline carbon films *Mater. Chem. Phys.* **96** 253–77

[31] Ferrari A C 2007 Raman spectroscopy of graphene and graphite: disorder, electron–phonon coupling, doping and nonadiabatic effects *Solid State Commun.* **143** 47–57

[32] Ferrari A C and Robertson J 2000 Interpretation of Raman spectra of disordered and amorphous carbon *Phys. Rev. B* **61** 14095

[33] ed Kumar C S 2012 *Raman Spectroscopy for Nanomaterials Characterization* (Berlin, Germany: Springer) DOI:10.1007/978-3-642-20620-7

[34] Ajtai T *et al* 2015 Microphysical properties of carbonaceous aerosol particles generated by laser ablation of a graphite target *Atmos. Meas. Tech.* **8** 1207–15

[35] Chys P, Gielens C and Meersman F 2011 FTIR 2D correlation spectroscopy of α1 and α2 fractions of an alkali-pretreated gelatin *Biochim. Biophys. Acta, Proteins Proteomics* **1814** 318–25

[36] Payne K J and Veis A 1988 Fourier transform IR spectroscopy of collagen and gelatin solutions: Deconvolution of the amide I band for conformational studies *Biopolymers* **27** 1749–60

[37] Yakimets I, Wellner N, Smith A C, Wilson R H Farhat I and Mitchell J 2005 Mechanical properties with respect to water content of gelatin films in glassy state *Polymer* **46** 12577–85

[38] Prystupa D and Donald A 1996 Infrared study of gelatin conformations in the gel and sol states *Polym. Gels Networks* **4** 87–110

[39] Polyak F and Reich G 2019 Infrared spectroscopic study of the coil-helix transition of highly concentrated gelatin formulations *Eur. J. Pharm. Biopharm.* **140** 11–19

[40] Manas E S, Getahun Z, Wright W W, DeGrado W F and Vanderkooi J M 2000 Infrared spectra of amide groups in α-helical proteins: Evidence for hydrogen bonding between helices and water *J. Am. Chem. Soc.* **122** 9883–90

[41] Shi X W, Yang X, Gaskell K J, Liu Y, Kobatake E, Bentley W E and Payne G F 2009 Reagentless protein assembly triggered by localized electrical signals *Adv. Mater.* **21** 984–8

[42] Wagner C, Naumkin A, Kraut-Vass A, Allison J, Powell C and Rumble Jr J 2007 *NIST X-ray Photoelectron Spectroscopy Database; NIST Standard Reference Database 20, Version 3.5 (Web Version)* (Gaithersburg: National Institute of Standards and Technology) DOI:10.18434/T4T88K

[43] Tyan Y C, Liao J D, Klauser R, Wu I D and Weng C C 2002 Assessment and characterization of degradation effect for the varied degrees of ultra-violet radiation onto the collagen-bonded polypropylene non-woven fabric surfaces *Biomaterials* **23** 65–76

[44] Chen Y, Schneider P and Erbe A 2012 Investigation of native oxide growth on zinc in different atmospheres by spectroscopic ellipsometry *Phys. Status Solidi* A **209** 846–53

[45] Wagner A J, Wolfe G M and Fairbrother D H 2003 Reactivity of vapor-deposited metal atoms with nitrogen-containing polymers and organic surfaces studied by in situ XPS *Appl. Surf. Sci.* **219** 317–28

[46] Guglielmelli A, Nemati S, Vasdekis A E and Sio L D 2018 Stimuli responsive diffraction gratings in soft-composite materials *J. Phys. D: Appl. Phys.* **52** 053001

[47] Zhang J *et al* 2019 Bio-responsive smart polymers and biomedical applications *J. Phys.: Mater.* **2** 032004

[48] Zhang L, Wang Z, Das J, Labib M, Ahmed S, Sargent E H and Kelley S O 2019 Potential-responsive surfaces for manipulation of cell adhesion, release, and differentiation *Angew. Chem. Int. Ed.* **58** 14519–23

[49] Assaf F, El-Rehiem S A and Zaky A 1999 Pitting corrosion of zinc in neutral halide solutions *Mater. Chem. Phys.* **58** 58–63

[50] Metikoš-Huković M and Milošev I 1992 Electrochemical methods in the study of localized corrosion attack *J. Appl. Electrochem.* **22** 448–55

[51] Mikić T K, Milošev I and Pihlar B 2005 Passivity and corrosion of Cu-xZn ($x = 10$–40 wt%) alloys in borate buffer containing chloride ions *J. Appl. Electrochem.* **35** 975–84

[52] Zhang X G 1996 *Corrosion and Electrochemistry of Zinc* (USA New York: Plenum Press) DOI:10.1007/978-1-4757-9877-7

[53] Miao W, Cole I S, Neufeld A K and Furman S 2007 Pitting corrosion of Zn and Zn-Al coated steels in pH 2 to 12 NaCl solutions *J. Electrochem. Soc.* **154** C7–C15

[54] Thierry D, Massinon D and Hugot-Le-Goff A 1991 In situ determination of corrosion products formed on painted galvanized steel by Raman spectroscopy *J. Electrochem. Soc.* **138** 879–80

[55] Marcus P and Herbelin J M 1993 The entry of chloride ions into passive films on nickel studied by spectroscopic (ESCA) and nuclear (^{36}Cl radiotracer) methods *Corros. Sci.* **34** 1123–45

[56] Zuo J and Erbe A 2010 Optical and electronic properties of native zinc oxide films on polycrystalline Zn *Phys. Chem. Chem. Phys.* **12** 11467–76

[57] Van der Leij M 1978 The possibility of black zinc oxide as spectrally selective coating for low temperature solar collectors *J. Electrochem. Soc.* **125** 1361–4

[58] Kegel J, Povey I M and Pemble M E 2018 Zno nanorod-arrays as photo-(electro)chemical materials: Strategies designed to overcome the material's natural limitations *J. Electrochem. Soc.* **165** H3034–H3044

[59] Liu Z, E L, Ya J and Xin Y 2009 Growth of ZnO nanorods by aqueous solution method with electrodeposited ZnO seed layers *Appl. Surf. Sci.* **255** 6415–20

[60] Sacco L, Florea I, Châtelet M and Cojocaru C S 2018 Electrical and morphological behavior of carbon nanotubes synthesized within porous anodic alumina templates *J. Phys.: Mater.* **1** 015004

[61] Wang Y, Wang X and Antonietti M 2012 Polymeric graphitic carbon nitride as a heterogeneous organocatalyst: from photochemistry to multipurpose catalysis to sustainable chemistry *Angew. Chem. Int. Ed.* **51** 68–89

[62] Masa J, Xia W, Muhler M and Schuhmann W 2015 On the role of metals in nitrogen-doped carbon electrocatalysts for oxygen reduction *Angew. Chem. Int. Ed.* **54** 10102–20

[63] Rombach M, Gelinsky M and Vahrenkamp H 2002 Coordination modes of aminoacids to zinc *Inorg. Chim. Acta* **334** 25–33

[64] Ashmead H D 2012 *Amino Acid Chelation in Human and Animal Nutrition* (Boca Raton, USA: CRC Press) DOI: 10.1201/b11533

[65] Brinckmann J, Notbohm H and Müller P 2005 *Collagen (Top. Curr. Chem.)* (Berlin: Springer) vol 247

[66] Guldi D M, Ramey J, Martínez-Díaz M V, dela Escosura A, Torres T, DaRos T and Prato M 2002 Reversible zinc phthalocyanine fullerene ensembles *Chem. Commun.* 2774–5

[67] Lin H Y, Cheng P Y, Wan C F and Wu A T 2012 A turn-on and reversible fluorescence sensor for zinc ion *Analyst* **137** 4415–17

[68] Aller Pellitero M and del Campo F J 2019 Electrochromic sensors: Innovative devices enabled by spectroelectrochemical methods *Curr. Opin. Electrochem.* **15** 66–72

[69] Jarosz T, Gebka K, Stolarczyk A and Domagala W 2019 Transparent to black electrochromism—the 'holy grail' of organic optoelectronics *Polymers* **11** 273